P1.50

Application of a Monte Carlo integration (MI) method to collision and coagulation growth processes of hydrometeors in a bin-type model

Yousuke Sato[1,5], Teruyuki Nakajima[1], Kentaroh Suzuki[2], and Takamichi Iguchi[3,4]

Corresponding author : Yousuke Sato, email : satoy@aori.u-tokyo.ac.jp

1 Atmosphere and Ocean Research Institute, The University of Tokyo, Kashiwa, Chiba, Japan

2 Department of Atmospheric Science, Colorado State University, Fort Collins, Colorado, USA

3 Earth System Science Interdisciplinary Center, University of Maryland, College Park, Maryland, USA

4 Laboratory for Atmospheres, NASA Goddard Space Flight Center, Greenbelt, Maryland, USA

5 Japan Society for the Promotion of Science, Chiyoda-ku, Tokyo, Japan

1. Introduction

Clouds, which cover about 70% of the earth's surface [*Rossow and Schiffer,* 1999], play a critical role in the atmosphere through various interaction processes such as latent heat release, radiation and water circulation. In particular, the recent attention of the climate research community to cloud perturbation by anthropogenic aerosols demands extensive simulations of detailed cloud microphysics. In such simulations, bin-type cloud models have been used to study the detailed modification of the size distribution of cloud droplets and aerosol particles [e.g., *Khain et al.*, 2005; *Lynn et al.*, 2005]. The satellite-derived signature of aerosol-cloud interaction with a significant reduction of the effective droplet radius has also been successfully simulated by these bin-type models [*Suzuki et al.*, 2006; *Iguchi et al.*, 2008].

The bin-type model, however, takes a large amount of computing time and is difficult to be used for simulation of large-scale areas and/or for many runs in sensitivity studies. So far the model has, therefore, been used only for idealized and meso-scale regional case studies [e.g., *Khain and Sednev,* 1996; *Takahashi and Kawano,* 1998; *Lynn, et al.,* 2005; *Iguchi et al.,* 2008].

Table 1 shows an example of CPU time taken by microphysical processes in the bin model of *Suzuki et al.* [2006]. The table indicates that more than 98% of the total CPU time is used by the condensation and the collision-coagulation processes, although the CPU time are different depending on the algorithms adopted by each bin-type model. In order to increase the computational efficiency, *Bott* [1998, 2000] proposed a flux method to reduce the numerical diffusion in the collision-coagulation processes by using a mass density distribution function, instead of the number density distribution function and using an accurate interpolation to solve the stochastic collision equation. *Suzuki* [2004] proposed a base function method to reduce the numerical diffusion by expanding the size distribution by a series of orthogonal functions. In spite of these improvements, the computational cost of bin-type models is still high.

In this paper, we propose a stochastic size- integration method for the collision-coagulation process of a bin type cloud model. And the purpose of this paper is to develop a numerically efficient method to approximate the traditional bin-method which is widely used by many researchers, in order to reduce the computation cost. We present the model description in section 2, calculation results in sections 3, 4, and 5 and the discussion in section 6.

2. Model description

The collision-coagulation growth of hydro- meteors in cloud is calculated by solving the stochastic collection equation (SCE) [e.g., *Pruppacher and Klett,* 1997; *Khain et al.,* 2000]:

$$\frac{\partial f(m)}{\partial t} = 2\int_0^{m/2} f(m')f(m-m')K(m',m-m')dm' \quad (1)$$
$$- f(m)\int_0^{\infty} f(m'')K(m,m'')dm''$$

where m is the mass of a hydrometeor particle, $f(m)$ is the number size distribution function (SDF) (number size concentration) and $K(m',m)$ is the collection kernel function determining the rate at which a particle of mass m' is collected by a particle of mass m. In order to solve (1), we adopt a logarithmically equidistant mass grid system following *Bott* [1998]. Following *Berry* [1967], a mass density function, $g(\eta)$, is introduced by:

$$g(\eta) = m^2 f(m), \qquad (\eta = \ln m) \qquad (2)$$

Substituting $g(\eta)$ into (1), the SCE of the mass density function is written as:

$$\frac{\partial g(\eta)}{\partial t} = 2\int_0^{\eta_1} \frac{m^2}{m_c^2 m'} g(\eta')g(\eta_c)K(\eta',\eta_c)d\eta', \qquad (3)$$
$$- \int_0^{\infty} g(\eta)\frac{K(\eta,\eta'')}{m''} g(\eta'')d\eta''$$

where $\eta_c = ln(m_c)$; $m_c = m - m'$; $\eta_1 = exp(\eta)/2$.

Collision of a particle at a grid point i (i-th bin), whose mass is m_i, with a particle at a grid point j (j-th bin), whose mass is m_j, yields a change in the mass density functions at the i-th and j-th bins, g_i and g_j. It also produces a new particle with mass $m' = m_i + m_j$. This process is calculated as follows:

$$g_i(i,j) = g_i - g_i \frac{K(i,j)}{m_j} g_j \Delta\eta\Delta t = g_i - \Delta g_i \qquad (4a)$$

$$g_j(j,i) = g_j - g_j \frac{K(i,j)}{m_i} g_i \Delta\eta\Delta t = g_i - \Delta g_j \qquad (4b)$$

$$g'(i,j) = \Delta g_i + \Delta g_j, \ (i,j = 1,2,\ldots,N_{bin}) \qquad (4c)$$

where Δg_i and Δg_j are the masses lost from i-th and j-th bins by collision, respectively, and $g_i(i,j)$ and $g_j(i,j)$ are values of the mass density function after the collision at the i-th and j-th bin, respectively. $g'(i,j)$ represents the total mass increase of the particle system identified as the new particle m' after the collision. $\Delta\eta$ is the grid spacing of the logarithmically equidistant mass grid system, Δt is the time interval for numerical integration and N_{bin} is the number of bins. Supposing that the new particle mass is in a k-th bin, i.e. $m_k < m' < m_{k+1}$, $g'(i,j)$ is decomposed into two contributions for *k-th* and *k+1-th* bins as in the scheme proposed by *Bott* [2000].

The traditional bin method evaluates all the collision combinations, ${}_{Nbin}C_2$, to solve (3) as follows:

$$\{g_l\}_{l=1,2,\cdots N_{bin}} = \sum_i^{N_{bin}-1}\sum_j^{N_{bin}} (\Delta g_i + \Delta g_j) \qquad (5)$$

On the other hand, in this study, we approximate (5) using a Monte-Carlo integration (henceforth abbreviated as MI) algorithm. This method does not calculate all combinations of bins, instead only some combinations are selected by uniform random numbers:

$$\{g_l\}_{l=1,2,\cdots N_{bin}} = \sum_{k_1=1,k_2=1}^{M} (\Delta g_{k_1} + \Delta g_{k_2}) \times w, \qquad w = \frac{{}_{N_{bin}}C_2}{M} \qquad (6)$$

where M is the number of selected bin combinations and w is a weighting factor to compensate for the lack of mass change caused by the reduced number of combinations. Computational efficiency is improved by introducing the factor w compared to the traditional bin method.

Equations (1), (5) and (6) assume collision and coagulation among particles of the same type of hydrometeor. We can extend these expressions to those for poly-dispersions for different types of hydrometeors, such as the seven hydrometeor types identified in the Hebrew University Cloud Model [*Khain and Sednev,* 1996] as follows:

$$\frac{\partial f^{(\lambda)}(m)}{\partial t} = \sum_\nu\sum_\mu 2\int_0^{m/2} f^{(\nu)}(m')f^{(\mu)}(m-m')K(m',m-m')dm' \qquad (7)$$
$$- f^{(\lambda)}(m)\sum_\sigma\int_0^{\infty} f^{(\sigma)}(m'')K(m,m'')dm''$$

$$\{g_l^{(\lambda)}\}_{l=1,2,\cdots N_{bin}}^{\lambda=1,2,\cdots N_{spc}} = \sum_\mu\sum_\nu\left[\sum_i\sum_j (\Delta g_i^{(\mu)} + \Delta g_j^{(\nu)})\right] \qquad (8)$$
$$\approx \sum_{\lambda_1=1,\lambda_2=1}^{L}\sum_{k_1=1,k_2=1}^{M}\left[(\Delta g_{k_1}^{\lambda_1} + \Delta g_{k_2}^{\lambda_2})\right] \times w$$
$$\left[w = \left(\frac{{}_{N_{bin}}C_2}{M}\frac{N_{spc}^2}{L}\right)\right]$$

where μ, ν, σ and λ represent the type of hydrometeor, N_{spc} is the number of hydrometeor types and L is the number of hydrometeor types selected in the

Monte-Carlo integration. The quadruplex integration in (7) is reduced to a double summation in (8), so that the MI introduces a significant benefit in the calculation time for the collision-coagulation process for poly-dispersions including different types of hydrometeors. In summary, the computational efficiency is improved by random bin selection with ratio of w_1 ($={}_{Nbin}C_2/M$) and also by hydrometeor type selection with ratio of w_2 ($=N_{spc}^2/L$). The total computation time is therefore reduced by the factor $R_{comp} = 1/\, w_1\, w_2$.

In case of large w, the size distribution in the next time-step can become negative when $g_i<\Delta g_i$ or $g_j<\Delta g_j$. In this case, we assure positive definiteness by the following procedure as proposed by *Bott* [1998].

$$g_i(i,j) = \max(g_i - \Delta g_i, 0)$$
$$g_j(j,i) = \begin{cases} \max(g_j - \Delta g_j, 0) & (i \neq j) \\ g_j - \Delta g_j & (i = j) \end{cases} \qquad (9)$$

Our method is also different from traditional bin method in terms of calculation order regarding hydrometeor types and sizes of hydrometeor. Traditional bin methods calculate interaction of different hydrometeor types and different sizes by collision with specific order [e.g. first, collision of liquid drop and ice particle, second liquid drop and snow particle, next, liquid drop and graupel etc.]. This can be invalid for collision process in nature if the natural collision process occurs randomly in terms of paring of colliding particles and types. In our MI, however, collision process is calculated by random order about hydrometeor type and size of hydrometeor because the order is selected by uniform random number. This may be more suitable to represent the stochastic nature of collision process in real clouds.

3. Results of numerical experiments with a box model

In this section, we show the results of numerical simulations with the present MI applied to a zero-dimensional box model, which calculates the development of SDF by only the collision-coagulation process. Simulated results are compared with the analytic solution of SCE [*Golovin*, 1963] and the results with Exponential Flux Method [*Bott,* 2000] (henceforth abbreviated as EFM). We also evaluate the computational cost and error of the MI.

For the test simulation, we integrate the SCE over the total time of 7200 s with a time interval of Δt= 1 s. The SDF is discretized by N_{bin} = 300 size-bins through uniformly dividing the logarithm of the hydrometeor's mass. Only one type of hydrometeor (water droplet) is considered. The initial size distribution is assumed to be the form of a gamma function:

$$f(m, t=0) = \frac{L'}{\overline{m}} \exp\left(-\frac{m}{\overline{m}}\right) \qquad (10)$$

where L' is the total cloud water content and $\overline{m}$ is the mean droplet mass. The mean radius of hydrometeor $\overline{r}$ can be defined as $\overline{m} = (4/3)\pi\rho\overline{r}^3$ where ρ is the density of water. We assume L' = 1 g m^{-3} and $\overline{r}$ = 10 μm in our simulation.

Figure 1a compares the MI result with the analytic solution for the Golovin kernel function $K(m',m) = (1.5\times 10^{-3})\times(m+m')$ [*Berry*, 1967]. It shows that the SDF obtained by the MI are not smooth functions of mass of hydrometeor but this non-smooth nature does not develop with time. The peak mode radii are same as those of analytic solution. And the maximum deviation from the analytic SDF at each time-step remains similar to that of traditional method (not shown). The root mean square error in the SDF over the total time becomes less than that of the traditional bin method when R ($=1/w_1$) is larger than 0.031.

Figures 1b and 1c compare the results of the MI with the EFM using a realistic kernel called the Hydro-dynamic Kernel:

$$K(m',m) = \pi\{r(m) + r(m')\}^2 |V(m) - V(m')| E_{col}(m,m') E_{coal}(m,m'), \qquad (11)$$

where $V(m)$ and $r(m)$ are the terminal velocity and radius of a hydrometeor whose mass is m, respectively, and E_{col} and E_{coal} represent the collection and coalescence efficiencies, respectively. In this case, the MI gives an appropriate SDF when R (= $1/w_1$ = $M/_{Nbin}C_2$) is in the range from 0.056 to 1 as shown in Figures 1b and 1c. However, growth of hydrometeor becomes delayed (see Fig. 1c) when R becomes as small as 0.031. A detailed study of the simulation results suggests that this delay begins when the compensation factor w in (6) becomes inadequately large, producing a significantly large value of $\Delta g_{i,j}$ which cannot be adequately corrected by (9). Therefore, R should be set as larger than 0.056 in the present MI.

Figures 2a and 2b show CPU time taken by the MI as a function of R and R_{spc}(= $1/w_2 = L/N_{spc}{}^2$). The figure shows that the CPU time changes in proportion to R and R_{spc}. When R is one, the CPU time of the present method is larger than that of the traditional bin method due to the cost of generating random numbers. When R is 0.056, which is the minimum value of R required for appropriate results, the CPU time is about 10% of traditional bin method.

4. Comparison with the traditional bin method using a two-dimensional model

We also performed two-dimensional simu- lations in order to compare the results from the MI and the traditional bin method. We selected two cases for simulation: a convective cloud case and a shallow stratus case generated by a warm bubble. We use a bin model developed by *Suzuki et al.* [2006, 2010a, 2010b]. The simulation domain is a two-dimensional area (x-z) of 30 km (dx = 0.5 km) in the horizontal direction and 15 km (dz = 0.2 km) in vertical direction for the convective cloud case, and 30 km (dx = 0.5 km) in horizontal and 5 km (dz = 0.05 km) in vertical direction for the stratus case. Initial conditions of wind shear, relative humidity and temperature as shown in Figure 3 are based on *Suzuki* [2004] for convective cloud and *Suzuki et al.* [2006] for stratus cloud, respectively. To trigger convection and cloud formation, a warm bubble is initially located as a potential temperature perturbation $\Delta\theta$ following *Gallus and Rancic* [1996]:

$$\Delta\theta = \Delta\theta_0 \left(\frac{\pi}{2} \sqrt{\left(\frac{x - x_0}{x_r}\right)^2 + \left(\frac{z - z_0}{z_r}\right)^2} \right), \qquad (12)$$

where x_0 = 9 km, z_0 = 1 km, x_r = 5 km, z_r = 1 km and $\Delta\theta$ = 1 K for the convective cloud case, and x_0 = 9 km, z_0 = 0.5 km, x_r = 5 km, z_r = 0.5 km and $\Delta\theta$ = 1 K for the stratus case. In the stratus simulation, we consider only warm processes because the cloud top temperature is always above 273 K. On the other hand, the convective cloud simulation is performed including the ice phase process with the seven types of hydrometeors, i.e., cloud droplet, ice crystals (plate, column, dendrite), snow, hail and graupel. First, we set R_{spc} = 1 and various R values from 1 to 0.056, and we take an ensemble average of five experimental results where R are same but the seeded random numbers are different. We integrate for 7200 s (two hours) with a time-step of Δt= 1 s. SDFs of hydrometeors are discretized into 60 size-bins [i.e. N_{bin}=60] by uniformly dividing the logarithm of the mass of hydrometeor. The range of hydrometeor size is defined as 3-3000μm. We call 3-30μm, 30-300μm, and 300-3000μm cloud, drizzle and rain water, respectively.

Figure 4 shows a snapshot of the cloud effective radius distribution for the convective cloud case 60 min after the start of the calculation. As expected from the previous tests, the present method gives results similar to the traditional bin method even if R is as small as 0.056. Figure 5 shows the relative error of the MI from the result of the traditional bin method. The mean error of each set of simulations changes exponentially with R. Relative errors of the effective radius of cloud,

$$r_e = \frac{\int_{r=3\mu m}^{r=30\mu m} r^3 f(r) dr}{\int_{r=3\mu m}^{r=30\mu m} r^2 f(r) dr}, \qquad (13)$$

and the accumulated amount of cloud water content, integrated from the initial time to the end of simulation, are about 3% and that of surface rain fall is less than 1% when R is 0.056.

Next, we change R_{spc} for a fixed R at 0.124. Figure 6 shows the accumulated amount of snow water content. When R_{spc} is less than one, the snow amount is either over- or underestimated, though it seems that there is no specific preference of R_{spc} values to cause either. The present method over/under-estimates all ice phase hydrometeors, including ice, graupel and hail amounts, though not shown. Such over/under-estimation is caused by a lack of mass transfer among some hydrometeor types in the MI. If R_{spc} is smaller than one, there are some types of hydrometeors for which collision and coagulation processes are not calculated. As a result, some types of hydrometeors grow more than by the traditional method, while another type does not grow fast enough. There are no preferred types and values of R_{spc} for over/under-estimation as shown in Figure 6 because hydrometeors for calculation are randomly selected. Figure 7 shows relative errors of the MI for various values of R_{spc}. The relative errors for all the hydrometeor types change exponentially with R_{spc}, as in the case of variable R.

Figures 8 and 9 show a snapshot of the effective radius distribution and the relative error as a function of R, respectively, in the stratus case at t = 60 min. As in the simulation of the convective cloud case, the present method obtains results similar to the traditional bin method even if R is 0.056 (Figure 8) and the relative error changes exponentially with R (Figure 9). Figure 10 shows the spatially averaged SDF (Mass density distribution) at 60 min after the start of simulation calculated by traditional bin and MI. These SDFs have complex forms with bi-modal feature. It is shown that the SDFs with $R=0.056$ and 0.124 have unsmoothed forms in second mode whereas the peak radii are same as the others, similar to the results with box model in section 3. This illustrates that the MI can also reproduce complex forms of SDF [e.g. bi-modal or tri-modal SDF] similar to traditional bin methods even for two dimensional cases.

Figure 11 shows the CPU time of the collision-coagulation process for the two-dimensional simulations. The slope of the fitted line for the stratus case (Figure 11b), 118 s, is smaller than 2291 s for the convective case (Figure 11a). This is because the collision and coagulation module is called more frequently in the convective case than in the stratus case, and also because, in convective cloud case, collisions between liquid particles and ice particles (e.g. ice crystals, snow, graupel and hail particles) are calculated since cloud top temperature of convective cloud is lower than 273 K. These results suggest that the more frequently the collision module is called, the stronger the benefit of the MI becomes in terms of the computational cost. For example, the MI is better for simulation of thick stratus clouds and deep convective clouds.

Furthermore, we evaluated how the simulation errors and standard deviations depend on the number of bins. We performed the same experiments as above but with 30 and 90 bins and compared the standard deviations and errors for the simulated cloud fields with those obtained from 60 bins. Figure 12 shows the error and the standard deviation of surface rainfall. The error has a similar trend regardless of the number of bins (Figure 12a), whereas the relative standard deviation decreases with the number of bins (Figure 12b).

5. Discussion

In the preceding sections, we studied the behavior of errors produced by the present MI in comparison with traditional bin method. In this section, we theoretically interpret the results shown above and further explore several aspects of the present method that would be beneficial for its potential applications in broader contexts.

5.1 Comparison of Monte-Carlo integration with aircraft data

We compared the computational errors with variability in aircraft observations that measure the SDF of clouds for investigating how comparable the numerical errors are to natural variabilities. This observed SDF is generally not a smooth function of a particle mass even if the cloud is relatively uniform. The non-smooth nature of the SDF reflects the fact that the cloud parameters observed in real atmosphere fluctuate spatially and temporally due to the turbulent structure of the cloud. In order to compare variability of cloud parameters between simulation and observation, a stratus simulation was performed using the present MI where variability of SDF in the results is caused by the random collision-coagulation process. The calculation domain is 30 km in horizontal (dx = 0.2 km) and 5 km in vertical (dz = 0.05 km). The integration time is one hour with a time-step of one second and R is set to 0.056. Initial conditions for temperature, horizontal wind and relative humidity are shown in Figure 13. Table 2 shows the spatially averaged mean and standard deviation of the effective radius by MI in comparison with the values for corresponding parameters obtained by aircraft data and by the traditional bin model. Aircraft data were obtained by B200 aircraft for the JACCS aircraft project, which equipped the Gerber's microphysics probe PVM-100A [*Gerber et al.*, 1994]. On 2 February 1998, B200 flew in a region of 29±1N, 128±1E with an average speed of about 80 m s^{-1}. Figure 14 shows effective radius of the aircraft observation data. The standard deviation of the effective radius from the MI is the same order as that of aircraft observation data. Also, the mean values and standard deviations of the effective radius obtained by the traditional bin method are almost same as those by the MI through cloud, drizzle and rain formation. These results demonstrate that both traditional bin and MI can represent dispersion of cloud parameters obtained by observation and that the random error generated by MI is much smaller than the variability included in the traditional bin model.

This finding suggests that the model dispersion is the result of internal instability caused by the dynamics of the cloud system itself that takes place in the real atmosphere, which is much larger than the random error generated by the MI. It can therefore be concluded that the dispersion caused by the present MI for the collision and coagulation process can be considered negligible compared to the natural variability in real atmosphere. This result supports the validity of the present MI. It would also be interesting to compare the SDFs calculated by the MI with those obtained from aircraft observations in terms of their randomness although such comparisons are difficult because observations always suffer errors in instrumentation as well as their random feature in nature.

This paper aims at development of a method to approximate the traditional bin scheme with focus on improvement of computational efficiency, and indeed demonstrated that the MI is as accurate as the traditional bin models that have been compared with SDF observations by many investigators [e.g., *Khairoutdinov and Korgan*, 1999]. Although the comparisons of the model with direct observations of SDF by aircraft is out of the scope of this paper, it is nevertheless worth noting that the natural cloud phenomenon with complicated size distribution functions cannot be fully reproduced even by traditional bin models as well as present MI. This is a common issue open for cloud modeling community, for which we should keep making efforts.

6. Conclusions

We proposed an application of the Monte Carlo integration procedure for the integration of the collision and coagulation equation of hydrometeor growth. This method reduces the computational cost of the collision and coagulation process to about 10% of that of the traditional method, thereby providing an efficient approximation of traditional bin method. This method employs uniformed random numbers, and it is shown that the results are dependent upon assumed random numbers. The random number principle causes some error, yet the error range of simulation results is found to be much less than internal variability that takes place in the real atmosphere.

Although the present study focused only on collision-coagulation processes, it is also important to reduce the computational costs for condensational growth process that is another bottle neck in cloud microphysical modeling as shown in Table 1. Several previous studies were devoted to this issue [e.g. *Bott*, 1989a 1989b; *Lowe et al.*, 2003; *Suzuki*, 2004; *Sugiura et al*. (personal communication)]. We will also investigate how our stochastic approach can be applied to the condensational growth processes in future studies.

References

Berry, E. X. (1967), Cloud droplet growth by collection, *J. Atmos. Sci.*, *24*, 688-701.

Bott, A. (1989a), A positive definite advection scheme obtained by nonlinear renomalization of the advective fluxes, *Mon. Wea. Rev.*, *117*, 1006-1015.

Bott, A. (1989b), Reply to comment on "A positive definite advection scheme obtained by nonlinear renormalization of the advective fluxes", *Mon. Wea. Rev.*, *117*, 2633-2636.

Bott, A., (1998), A flux method for the numerical solution of the stochastic collection equation, *J. Atmos. Sci.*, *55*, 2284-2293.

Bott, A. (2000), A flux method for the numerical solution of the stochastic collection equation:extension to two-eimensional particle distributions, *J. Atmos. Sci.*, *57*, 284-294.

Gallus, W. A. Jr., and M. Rancic (1996), A non-hydrostatic version of the NMC's regional Eta model, *Quart. J. Roy. Meteor. Soc.*, *122,* 465-497.

Gerber, H., B.G. Arends, and A.S. Ackerman (1994), New microphysics sensor for aircraft use, *Atmos. Research*, *31*, 235-252.

Golovin, A. M. (1963), The solution of the coagulation equation for cloud droplets in a rising air current., *Bull. Acad. Sci., USSR, Geophys. Ser. X*, *5*, 482-487.

Iguchi, T., T. Nakajima, A.P. Khain, K. Saito, T. Takemura, and K. Suzuki (2008), Modeling the influence of aerosols on cloud microphysical properties in the east Asia region using a mesoscale model coupled with a bin-based cloud microphysics scheme., *J. Geophys. Res.*, *113*, D14215, doi:10.1029/2007JD009774.

Khain, A. P., and I. Sednev (1996), Simulation of precipitation formation in the eastern Mediterranean coastal zone using a spectral microphysics cloud ensemble model, *Atmos. Res.*, *43*, 77-110, doi:10.1016/ 0169-8095(96) 00005-1.

Khain, A. P., M. Ovtchinnikov, M. Pinsky, A. Plkrovsky, and H. Krugliak (2000), Notes on the state-of-the-art numerical modeling of cloud microphysics, *Atmos. Res.*, *55*, 159-224.

Khain, A., D. Rosenfeld, and A. Pokrovsky (2005), Aerosol impact on the dynamics and microphysics of deep convective clouds, *Q. J. R. Meteorl. Soc.*, *131*, 2639-2663, doi: 10.1256/qi.04.62

Khairoutdinov, M. F., Kogan, Y. L. (1999), A Large Eddy Simulation Model with Explicit Microphysics: Validation against Aircraft Observations of a Stratocumulus-Topped Boundary Layer., *J. Atmos. Sci.*, *56,* 2115-2131.

Liu, Y., and P. H. Darm (2004), Parameterization of the Autoconversion Process. Part I: Analytical Formulation of the Kessler-Type Parameterizations., *J. Atmos. Sci.*, *61*, 1539-1548.

Liu, Y., P. H. Darm, R. L. McGraw, M. A. Miller, and S. Niw. (2007), Theoretical expression for the autoconversion rate of the cloud droplet number concentration, J. *Geophys. Res. Lett.*, *34*, doi:10.1029/2007GL030389.

Lowe, D., A. R. MacKenzie, N. Nikiforakis, and J. Kettleborough (2003), A condensed-mass advection based model for the simulation of liquid polar stratospheric clouds, *Atmos. Chem. Phys.*, *3*, 29-38.

Lynn, B. H., A. P. Khain, J. Dudhia, D. Rosenfeld, A. Pokrovsky, and A. Seinfert (2005), Spectral (bin) microphysics coupled with a mesoscale Model (MM5). Part I: Model description and first results, *Mon. Wea. Rev.*, *133*, 44-58.

Prupacher, H., and J. D. Klett (1997), *Microphysics of Clouds and Preccipitation.*, 2nd ed., 954 pp., Springer, New York.

Rogers, R. R., and M. K. Yau (1989), *A short course in cloud physics*, 3rd ed. 293 pp., Pergamnon Press, Oxford.

Rossow, W. B., and R. A. Schiffer, (1999), Advances in understanding clouds from ISCCP, *Bull. Amer. Meteorol. Soc.*, *80*, 2261-2287.

Saito, K., T. Fujita, Y. Yamada, J. Ishida, Y. Kumagai, K. Aranami, S. Ohmori, R. Nagasawa, S. Kumagai, C. Muroi, T. Kato, H. Eito, and Y. Yamazaki (2006), The operational JMA nonhydrostatic mesoscale model, *Mon. Wea. Rerv.*, *134*, 1266-1298.

Seifert, A., A. Khain, A. Pokrovsky, and K. D. Beheng (2006), A comparison of spectral bin and two-moment bulk mixed-phase cloud microphysics, *Atmos. Res.*,*80*, 46-66.

Suzuki, K. (2004), A study on numerical modeling of cloud microphysics for calculating the particle growth process, Ph.D thesis, Univ. Tokyo, Tokyo, Japan.

Suzuki, K., T. Nakajima, T. Y. Nakajima, and A. Khain (2006), Correlation Pattern between Effective Radius and Optical Thickness of Water Clouds Simulated by a Spectral Bin Microphysics Cloud Model., *SOLA*, *2*, doi:10.2151/sola.2006-030.

Suzuki, K., T. Nakajima, T. Y. Nakajima, and A. P. Khain (2010a), A study of microphysical mechanism for correlation pattern between droplet radius and optical thickness of warm cloud with spectral bin microphysics cloud model., *J. Atmos. Src.*, 67, 1126-1141.

Suzuki, K., T. Nakajima, T. Y. Nakajima, and G. L. Stephens (2010b), Effect of the droplet activation proess on microphysical properties of warm clouds., *Environ. Res. Lett.*, 5, doi:10.1088/1748-9326/5/2/024012.

Takahashi, T., and T. Kawano (1998), Numerical Sensitivity Study of Rainband Precipitation and Evolution, *J. Atmos. Sci.*, *55*, 57-87.

Table

Table 1. Example of the CPU times (s) and contributions to the total time (%) for calculation of cloud microphysics processes by a bin-type model.

Process	CPU time (s)	Contribution to total time (%)
Nucleation	2.98	0.3
Freezing, Melting	3.45	0.3
Condensation	808.39	70.9
Collision-Coagulation	325.13	28.5
All	1139.95	100

Table 2. Values of effective radius and its standard deviation calculated by each model and obtained by aircraft data. In the simulation, t = 25 min, 30 min and 45 min correspond to the time for cloud, drizzle and rain formation, respectively.

Model/Measurement	Effective Radius [μm]	Standard deviation
MI (t = 25 min)	11.776	0.30504
Traditional bin (t = 25 min)	11.778	0.30505
MI (t = 30 min)	11.719	0.43937
Traditional bin (t = 30 min)	11.724	0.43915
MI (t = 40 min)	9.2868	0.66117
Traditional bin (t = 40 min)	9.3037	0.66107
Aircraft	10.753	0.20896

Figure

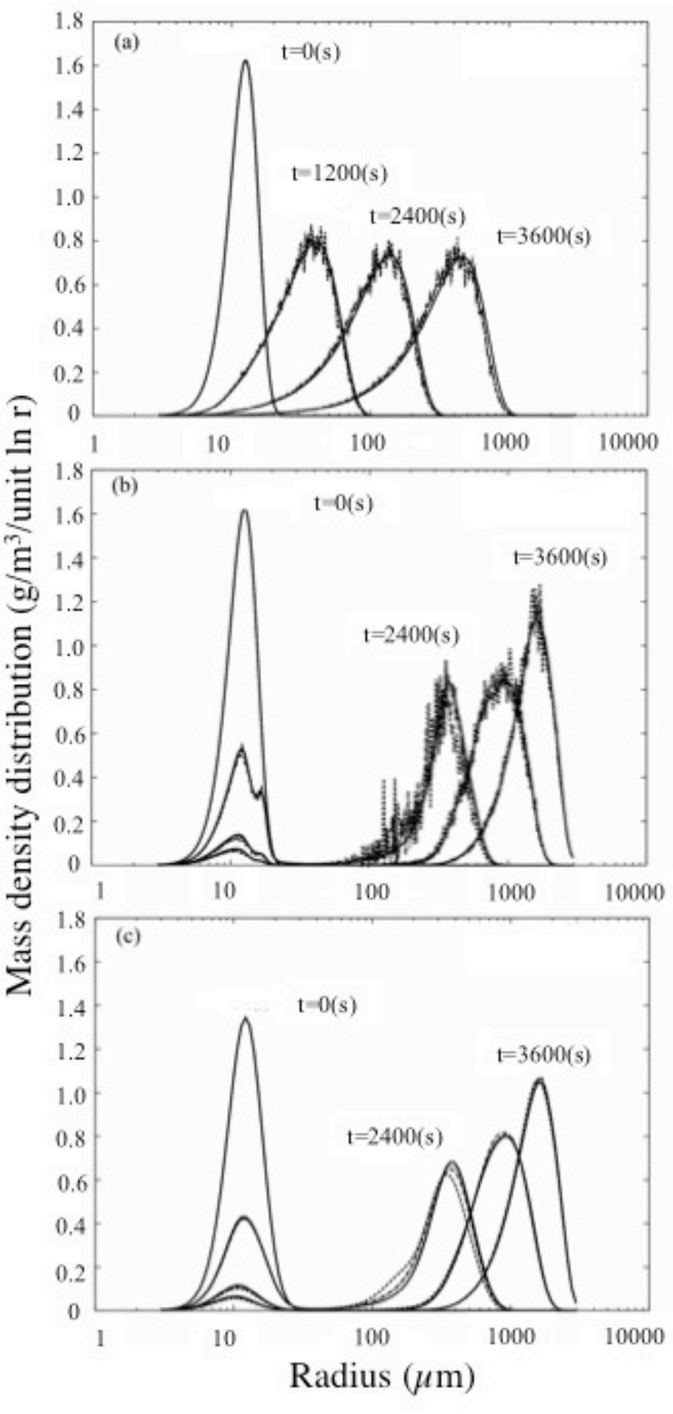

Figure 1. Time evolution of the mass density size distribution (SDF) (a,b) and the smoothed result of b (c). Panel (a): Solid line represents the analytic solution of SCE [*Golovin*, 1963] and dashed lines and dot-dashed lines represent the numerical results obtained by the MI with R = 0.031 and 0.125, respectively. Panels (b) and (c): Solid lines represents the numerical results obtained by the traditional bin method, and dashed lines, dash-dotted lines, and dotted lines represent those obtained by the MI with R = 0.031, 0.056, and 0.125, respectively.

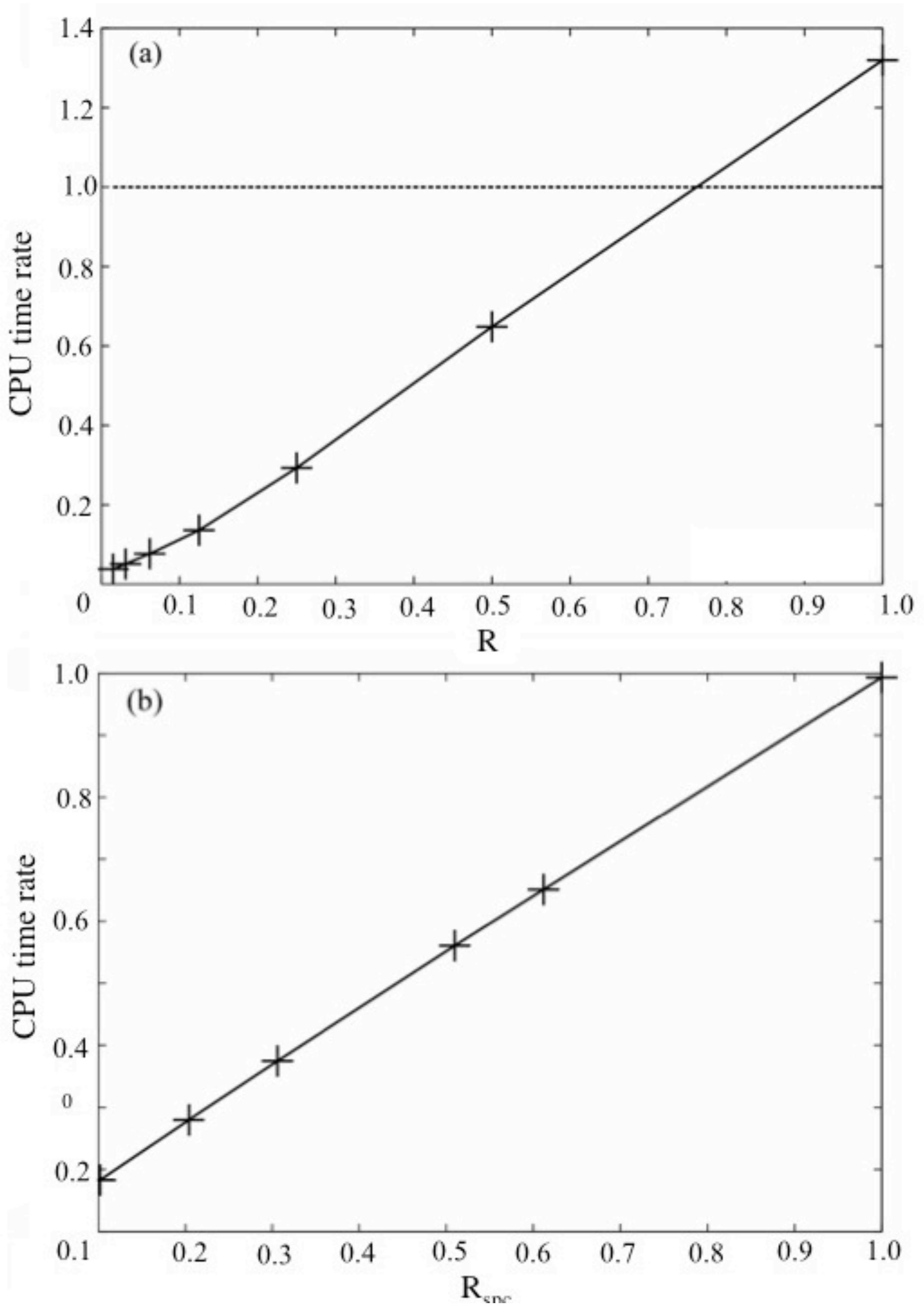

Figure 2. CPU times for the collision-coagulation processes, normalized by the CPU time for the traditional bin method, as functions of (a) *R* and (b) R_{spc}. Solid lines and dots are CPU times taken by the MI, and dotted lines are those for the traditional bin method.

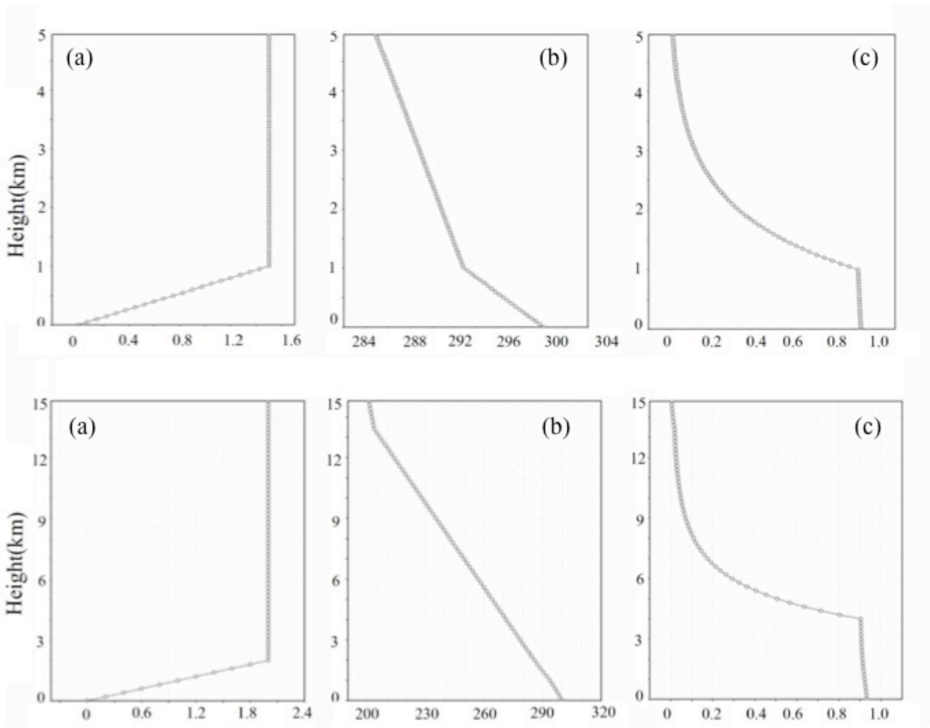

Figure 3. Initial conditions for atmospheric dynamics assumed for the two-dimensional numerical experiments. (a: Horizontal wind, b: temperature and c: relative humidity). The upper figure is for a stratus case and the lower figure is for a convective cloud case.

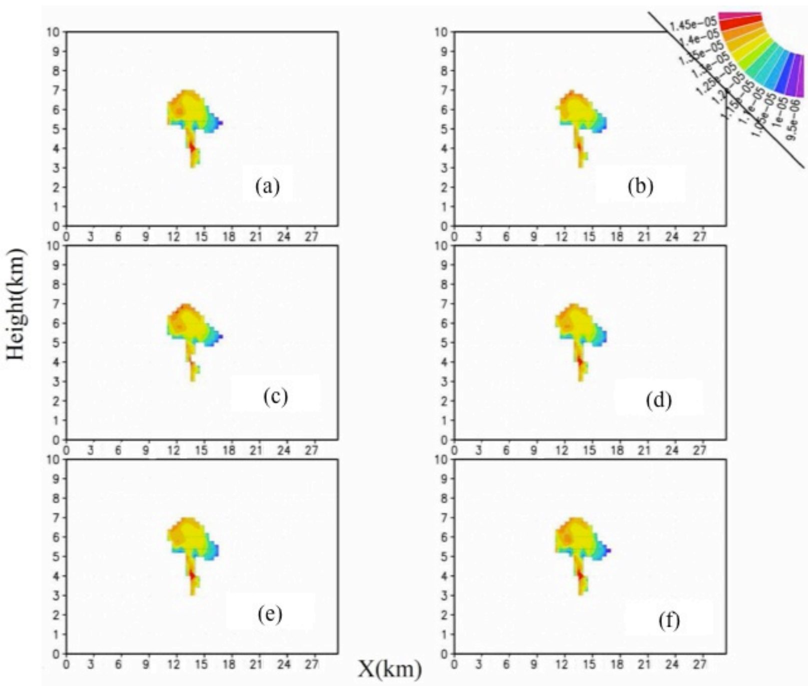

Figure 4. Horizontal distance-height sections of the cloud effective radius distribution formed by a warm bubble at t = 60 min in the convective cloud case for R_{spc} = 1 and various values of R. The panel (a) represents the result of the traditional bin model and other panels represent MI with (b) R=0.056, (c) R=0.124, (d) R=0.25, (e) R=0.5, and (f) R=1.

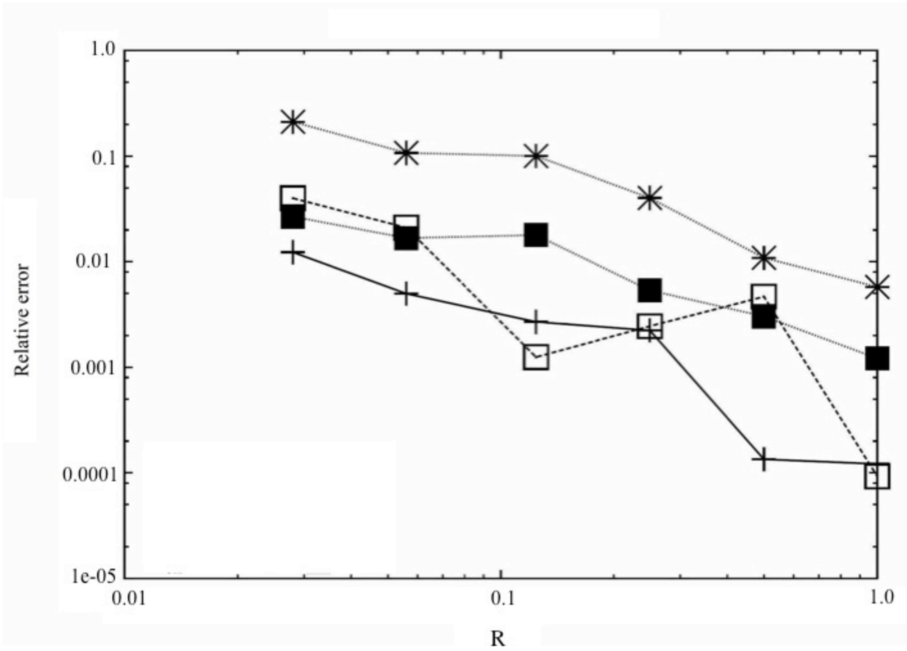

Figure 5. Relative errors of the MI averaged over the whole simulation domain for time-integrated amounts of surface rain (----+----), cloud water content (----□----), snow water content (----∗----), and effective radius (----■----) at t = 60 min.

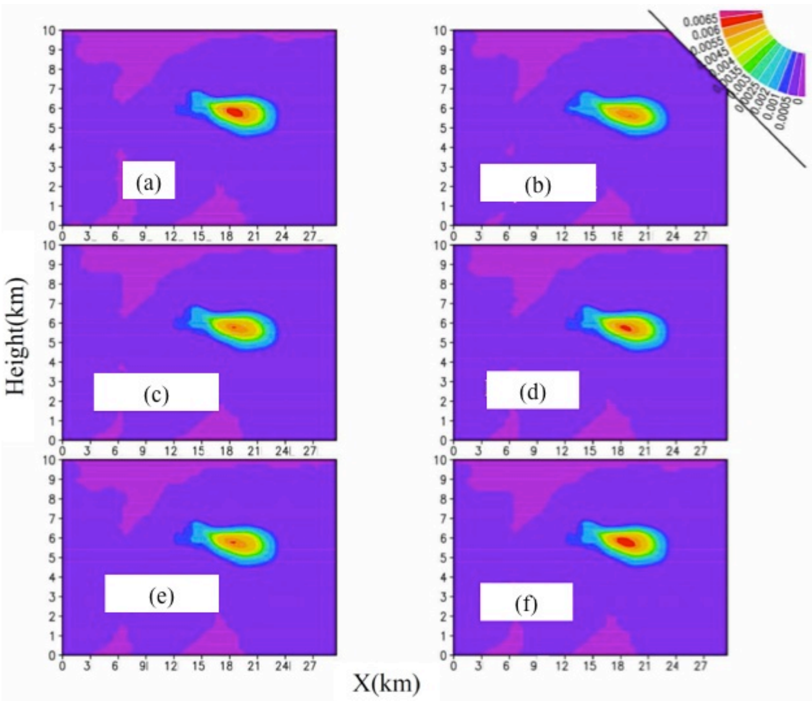

Figure 6. Horizontal distance-height sections of the amount of the snow water content integrated from t = 0 to the end of the calculation. Results for different values of R_{spc} are shown. The panel (a) represents the result of the traditional bin model and other panels represent the result from MI with (b) R_{spc}=0.204, (c) R_{spc}=0.306, (d) R_{spc}=0.51, (e) R_{spc}=0.612, and (f) R_{spc}=1.

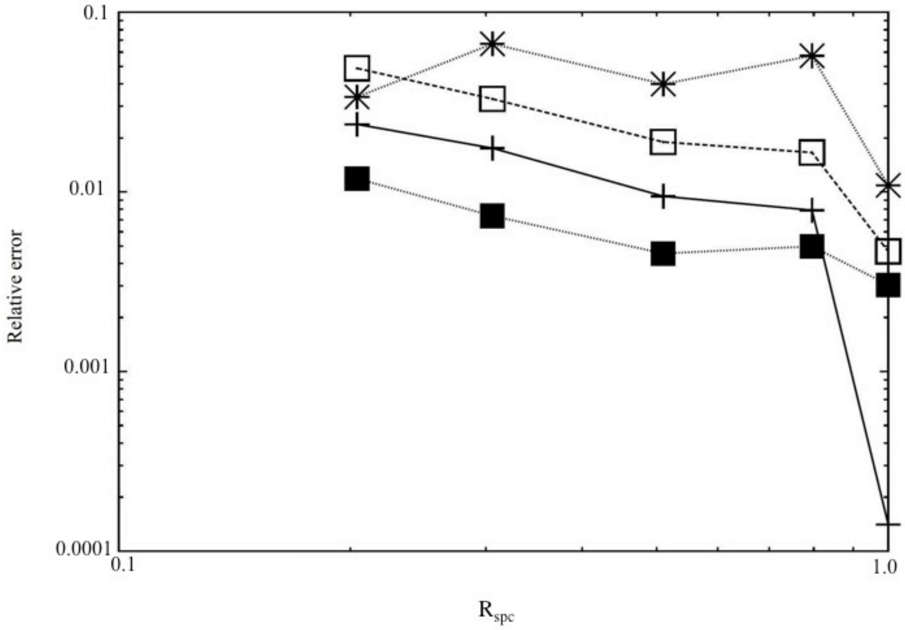

Figure 7. Same as Figure 5, but for results with various R_{spc} and R = 0.124.

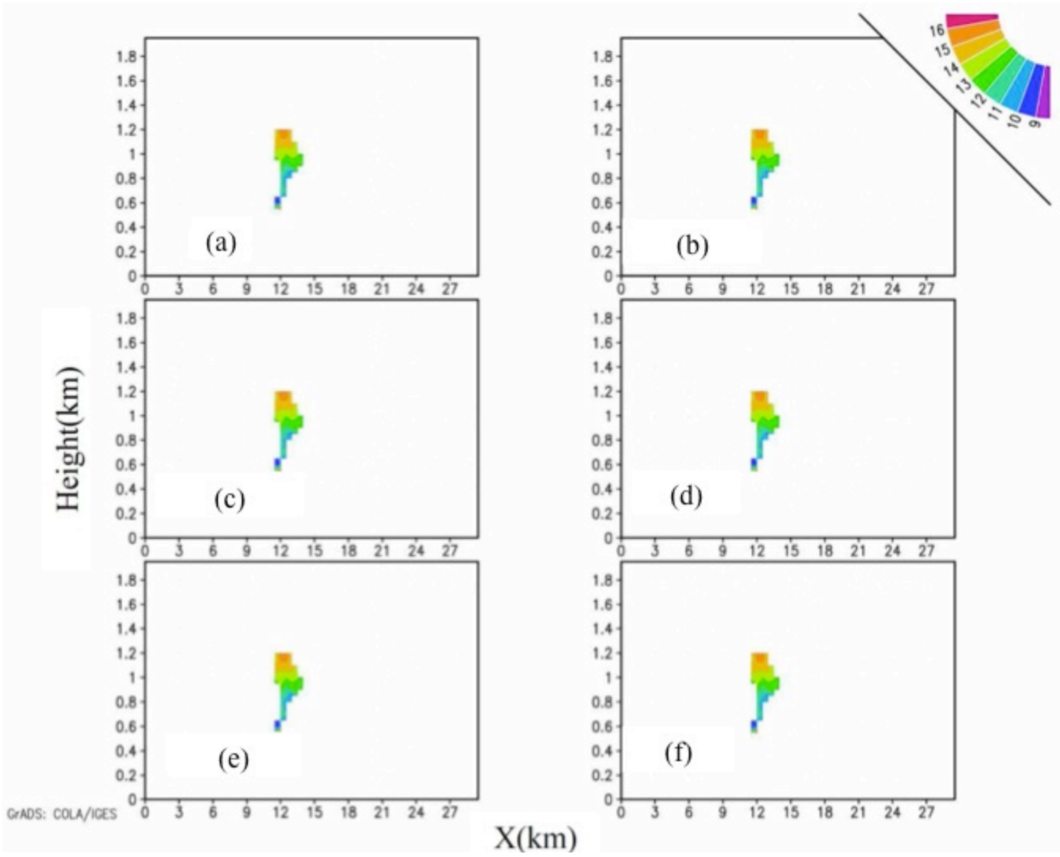

Figure 8. Same as Figure 4, but for the stratus case.

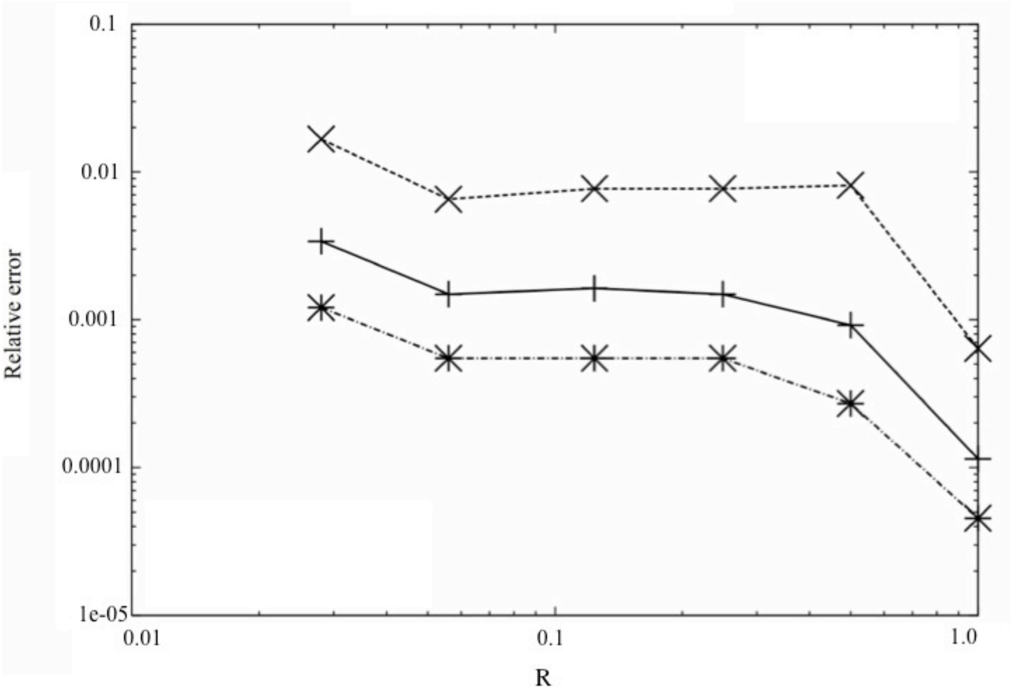

Figure 9. Same as Figure 5, but for the stratus case. Time integrated amount of cloud water content(----+----), drizzle water content (---＊----), and effective radius at t= 60 min(----×----).

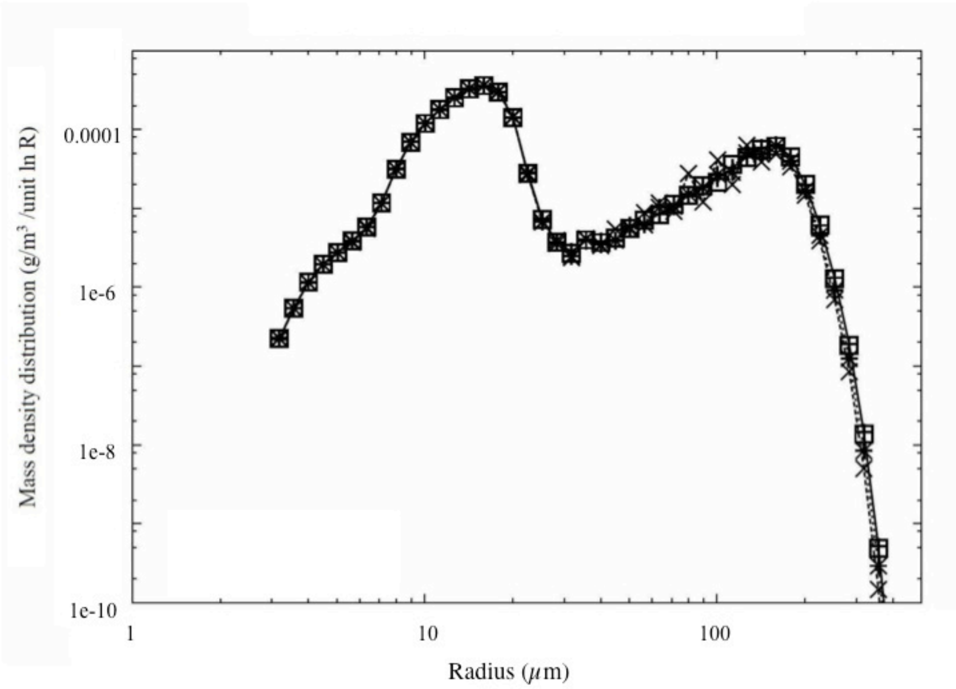

Figure 10. Spatially averaged mass density distribution (SDF) spectra [averaged the spectra of the grid in which complex form of spectra are calculated] in stratus condition calculated by traditional bin (----+----) and our new method with *R=0.056*(----×----), *0.124*(----＊----), *0.5*(----□-----).

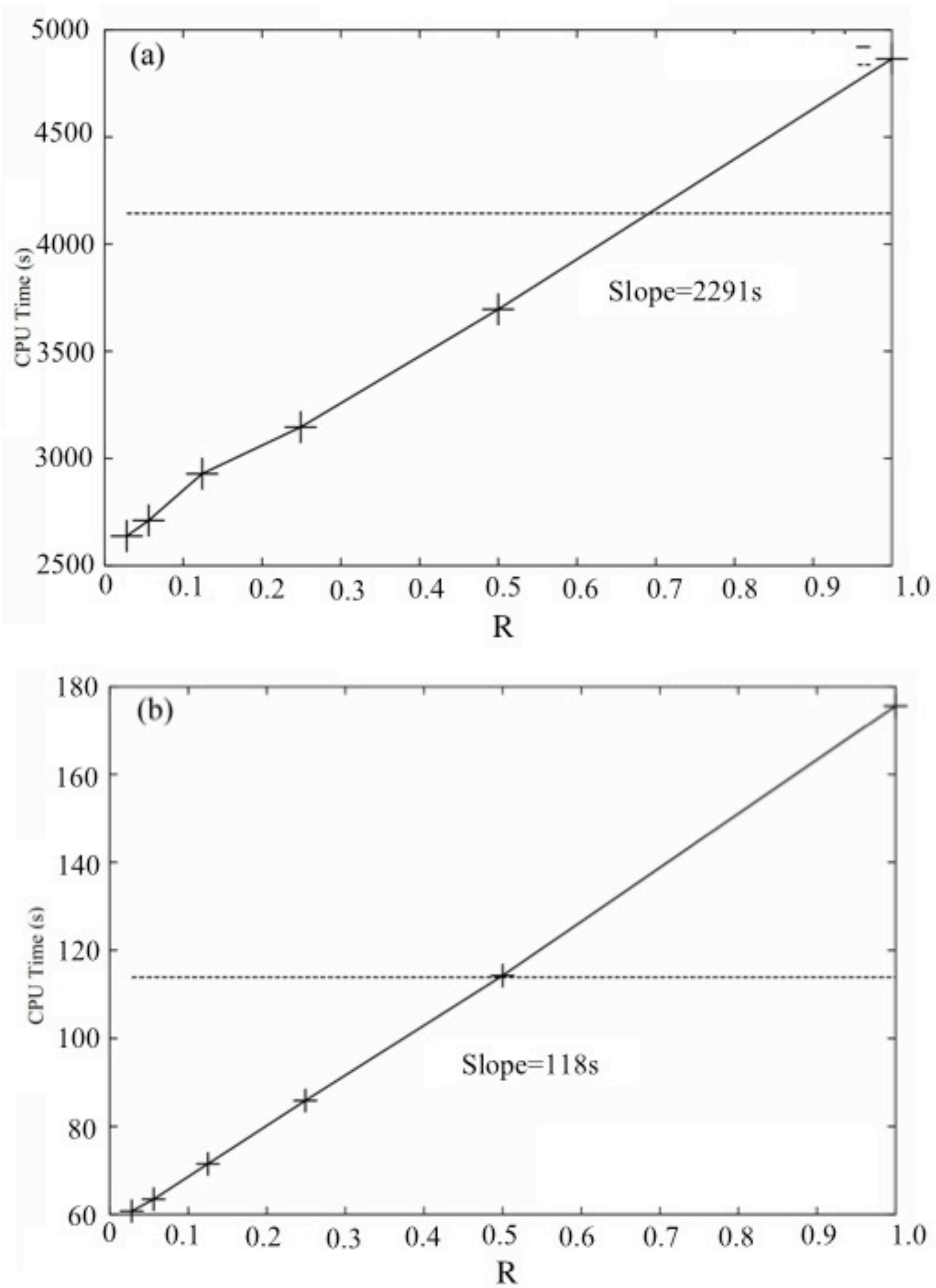

Figure 11. CPU time taken by the cloud microphysical module for the two-dimensional model simulation: CPU time in the (a) stratus case and (b) convective cloud case. CPU times for the MI (---+----), and for the traditional bin method (------).

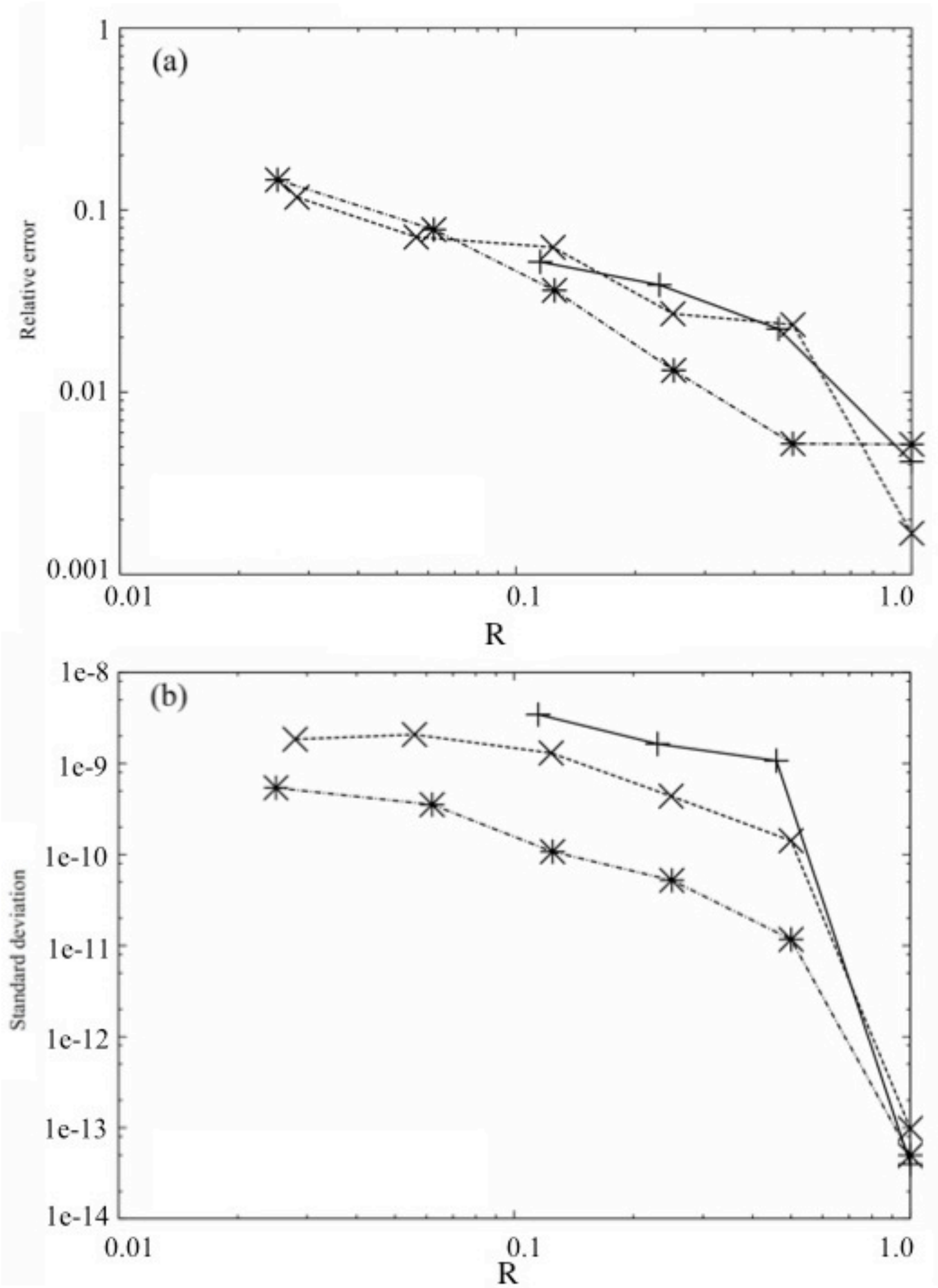

Figure 12. Errors and standard deviation of surface rain obtained by MI for various number of bins: error in the (a) and standard deviation in the (b). 30 bin (----+----), 60 bin (---X----), and 90 bin (----＊----) .

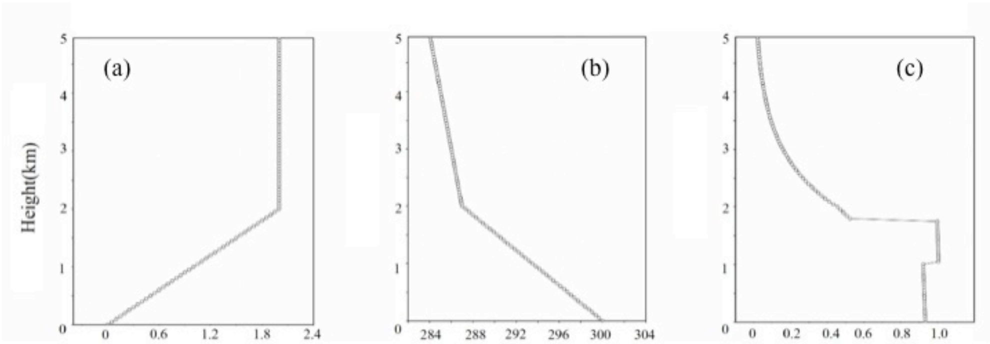

Figure 13. Initial conditions for atmospheric dynamics assumed for the two-dimensional numerical experiments. (a: horizontal wind, b: temperature, and c: relative humidity).

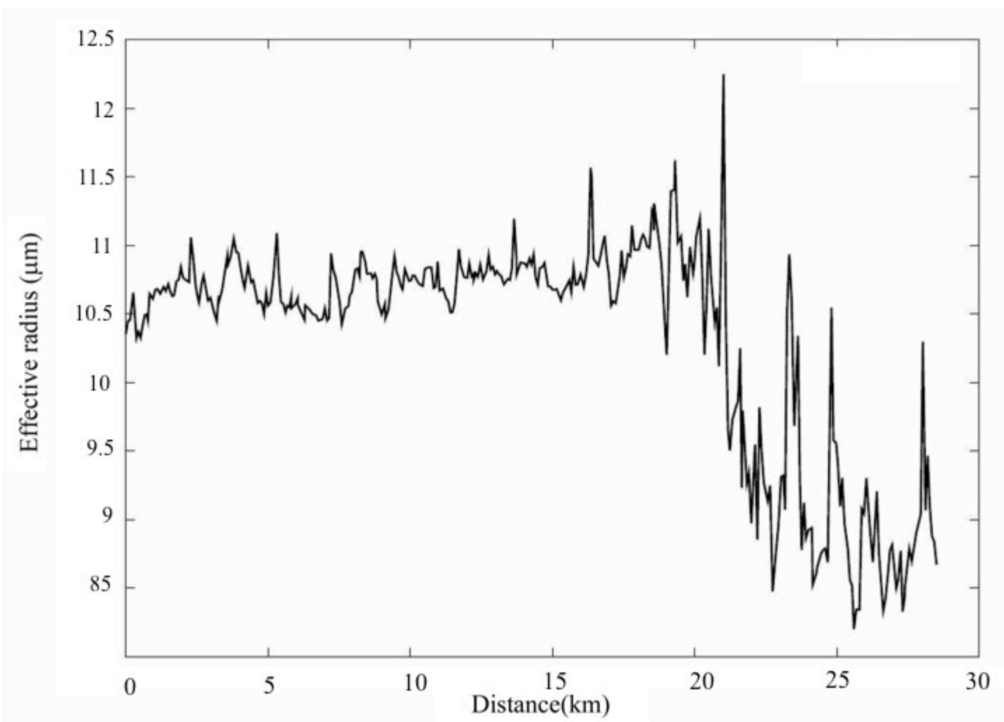

Figure 14. Values of effective radius as a function of the flight distance of B200 aircraft in the observation on 2 February 1998.